A Combined Computational Fluid Dynamics (CFD) and Experimental Approach to Quantify the Adhesion Force of Bacterial Cells Attached to a Plane Surface

Benjamin Boulbene, Jérôme Morchain and Muriel Mercier Bonin
Université de Toulouse, INSA, UPS, INP, LISBP, Toulouse F-31077, France

INRA, UMR792, Ingénierie des Systèmes Biologiques et des Procédés, Toulouse F-31400, France

CNRS, UMR5504, Toulouse F-31400, France

Sébastien Janel and Frank Lafont
CMIP-Institut Pasteur de Lille, CNRS UMR8204, INSERM U1019, Univ. Lille Nord de France, Lille F-59021, France

Philippe Schmitz
Université de Toulouse, INSA, UPS, INP, LISBP, Toulouse F-31077, France

INRA, UMR792, Ingénierie des Systèmes Biologiques et des Procédés, Toulouse F-31400, France

CNRS, UMR5504, Toulouse F-31400, France

DOI 10.1002/aic.13747
Published online February 8, 2012 in Wiley Online Library (wileyonlinelibrary.com).

A three-dimensional model is developed to study the laminar shear flow past a bacterial cell attached to a plane surface. The induced hydrodynamic forces and torque exerted on the cell are computed to clarify the prevailing mechanisms involved in the detachment of model bacteria. Results are discussed in terms of drag and torque magnitude as a function of the angles defining the orientation of the cell. It is shown that reorientation and rolling of spheroid-shaped cells are favored. It is also confirmed that rod-shaped cells would tend to lie on the surface and become aligned with the flow. The model is used to quantify the adhesion force of spheroid Bacillus cereus *spores to stainless steel, deduced from previously described experiments in a shear stress flow chamber. The magnitude of the predicted adhesion force is close to that obtained using atomic force microscopy under similar experimental conditions.* © 2012 American Institute of Chemical Engineers *AIChE J,* 58: 3614–3624, 2012
Keywords: bacterial adhesion, shear flow, hydrodynamics, model

Introduction

Microbial adhesion to surfaces followed by cell growth and colonization results in the formation of an extracellular polymeric matrix capable of protecting the underlying microorganisms from antimicrobials, chemical biocides, and host defense mechanisms.[1,2] Biofilms are ubiquitous and known to play an important role in a wide variety of environments, including biomedical implants,[1] wastewater plants,[2] marine,[3] and food-processing equipment.[4] Harsh cleaning and disinfecting procedures are generally carried out to control the growth of sessile microorganisms, based on a combination of chemical and thermomechanical effects. When a Cleaning-In-Place strategy is required, both the mean turbulent flow and the associated velocity fluctuations have been proved to play a major role in bacterial removal.[5,6] Beyond these curative methods, one way to limit biofilm formation is to prevent the adhesion of individual microorganisms, which generally constitutes the first step of surface colonization.[7] To this end, numerous works have been devoted to the modification of the material structure or chemistry to achieve nonadhesive and biocide properties, like, for instance, nanocomposite thin films.[8–10] Chemical additives could also be used with a view to limiting the physicochemical interactions between attached microorganisms and solid surfaces. Other studies focus on the characterization of the physicochemical properties of the bacterial surface, in relationship with the adhesion strength.[11–13]

Whatever the field of investigation, precise quantification of the adhesion force is required. Various types of apparatus have already been described in the literature for microbial adhesion-targeted applications: atomic force

Correspondence concerning this article should be addressed to P. Schmitz at philippe.schmitz@insa-toulouse.fr.

microscopy (AFM),[14] optical tweezer,[15] and shear stress flow chamber.[16–21] The last provides an indirect method for estimating the adhesion force under hydrodynamic conditions similar to the mean flow conditions experienced in industrial cleaning processes. Although the shear stress flow chamber appears to be a simple, convenient, and accurate device, it must be carefully designed to give a fully developed laminar two-dimensional (2-D) Poiseuille flow.[22] All individual biological entities attached to the bottom surface of the flow channel are thus exposed to constant and identical hydrodynamic stresses. Therefore, the complex theoretical problem can be simplified as the ideal case of a laminar infinite linear shear flow over a single cell in contact with an infinite plane wall at rest. In the case of a spherical particle, an analytical solution for the forces and torque was established by O'Neill[23] and Krishnan and Leighton.[24] However, the shear stress flow chamber is widely used in studies devoted to analyzing the adhesion of various biological particles (bacteria, yeast cells, and spores), the shape of which differs significantly from a sphere. In the absence of an exact quantification of the forces and torque exerted on the cells, the conclusions of these works are often limited to a purely qualitative comparison. Several numerical studies have already focused on the calculation of shear-induced stresses on a cell to improve the understanding of its detachment.[25–30] Gaver and Kute[28] studied the influence of the cell size to channel height ratio, through a 2-D model. Brooks and Tozeren[31] developed their own code and performed a three-dimensional (3-D) simulation of the flow over an array of cells of various shapes (sphere, hemisphere, and sphere with protrusion). Some works have highlighted the interesting phenomenon of reorientation of nonspherical cells attached to a surface under shear flow,[26,29] but neither the displacement nor the stresses were quantified.

In this article, we propose to determine the hydrodynamic forces and torque on nonspherical bacteria attached to a flat surface through a numerical simulation of the 3-D flow field. To this end, the commercial software COMSOL Multiphysics is used to compute the flow field past a single cell adhering to the channel bottom plate. The resolution of the flow allows a precise quantification of the velocity and pressure fields at the cell surface. These are further used to calculate the stresses exerted on the cell. Different characteristic shapes of microorganisms (sphere, spheroid, and rod) are investigated. In the last two cases, the influence of the incident flow direction, relative to the symmetry axis of the cell, is studied. The simulation procedure is first validated through a comparison of the computed hydrodynamic stresses with the analytical solutions valid for a spherical particle at low Reynolds number.[23,24] Simulations performed with a spheroid-shaped cell are then used with a view to interpreting, in terms of adhesion force, shear flow induced detachment experiments of *Bacillus cereus* spores attached to stainless steel.[32] Moreover, independent and direct measurements using AFM under the same experimental conditions (type of strain and solid surface, physicochemical parameters) are presented to confirm that the methodology proposed here allows a fair estimation of the adhesion force. The hydrodynamic forces and torque exerted over a rod-shaped bacterium, obtained numerically, are further investigated as a function of its position on the surface. All cases from the vertical to the horizontal position are carefully examined.

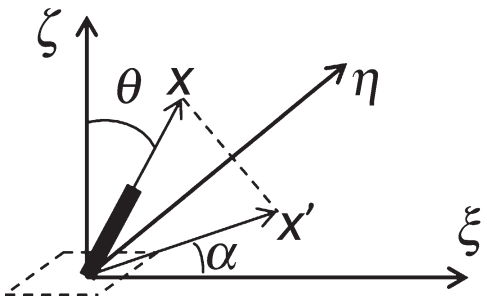

Figure 1. Definition of the cell position in the main coordinate system.

Theoretical Background

Model system

We are especially interested in computing the laminar flow past an individual bacterial cell attached to the bottom plate of a channel. The channel is rectangular and is in the region of the shear stress flow chamber where a fully developed stationary 2-D Poiseuille flow takes place. The subsequent hydrodynamic forces and torque exerted on the cell will then be calculated from the velocity and pressure fields obtained numerically. The model bacterium takes characteristic shapes (sphere, spheroid, and rod) to account for various cell morphologies generally encountered in biofilm-associated applications. All these shapes present an axis of revolution, named x. An orthogonal coordinates system (ξ, η, ζ) attached to the plane surface is used to characterize the flow direction relative to the cell; the ξ-direction is that of the incident flow. The position of the model bacterium can be defined by two angles. α is the angle between the main flow direction (axis ξ) and the projection, x', of the revolution axis of the cell (axis x) on the $\eta\xi$ plane. The zenith angle, θ, is the angle between the vertical axis ζ and the x axis. It is equal to 0 when the bacterium is in the vertical position and equal to $\pi/2$ when it is lying on the plane surface (see Figure 1).

The parameter defining the sphere is its radius r, the spheroid (or ellipsoid of revolution) is defined using its equatorial radius r_a and polar radius r_b ($r_b > r_a$). The contact area between the cell and the surface is defined taking a virtual embedment, l, of the cell inside the bottom plate (see Figure 2a). An orthogonal coordinates system (x, y, z) is attached to the cell: its origin is the cell center and the x-direction is the revolution axis of the cell. The two coordinate systems and angle α are represented in Figure 2b.

The parameters for the rod-shaped bacterium are its length, b, and its radius, r (Figure 2c). The definition of the coordinates system is slightly different in the present case: the origin (x, y, z) is the center of rotation of the cell referenced by point O. Its projection on the $\eta\xi$ plane defines the origin of the (ξ, η, ζ) coordinate system. The two coordinate systems and the two angles α and θ are represented in Figure 2d.

Fluid flow

As we focus on a single cell, the region of interest for the flow is the vicinity of the cell, that is, the near-wall region where the macroscopic Poiseuille flow is locally disturbed by the presence of the cell. To perform a study using a range of incident angles, it is convenient to select a unique computational domain that will be kept whatever the incident flow

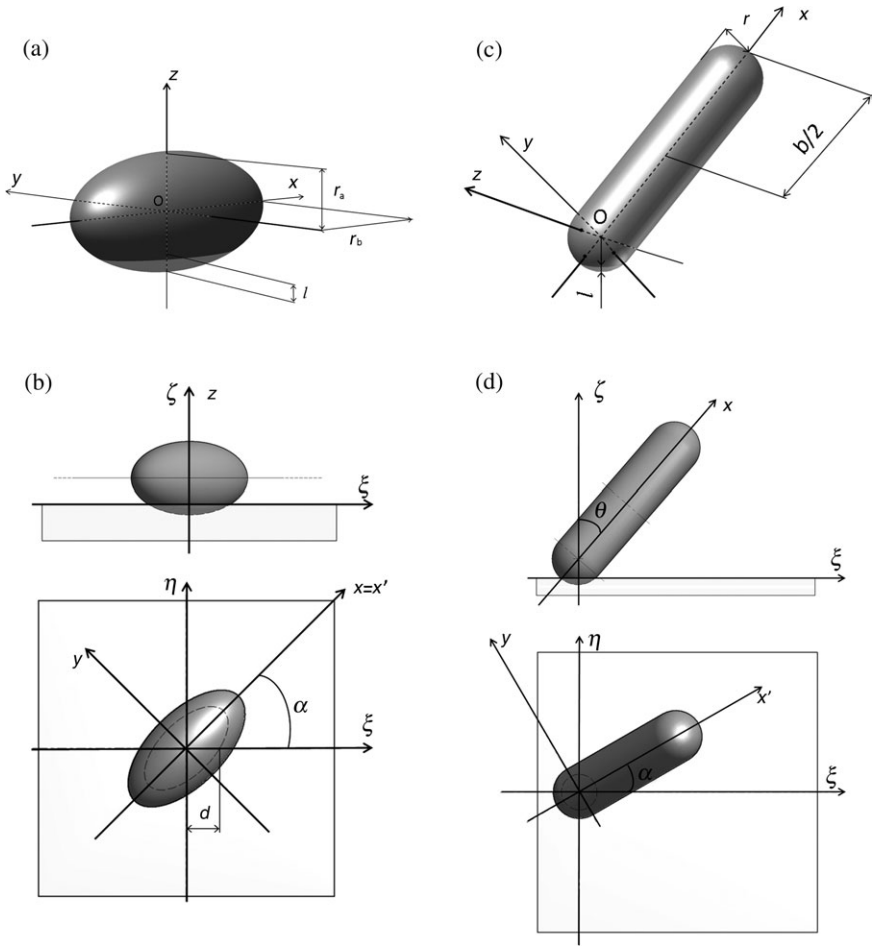

Figure 2. Detailed representation of the cell shape and position: spheroid-shaped cell model (a and b) and rod-shaped cell model (c and d).

direction. This is done by choosing the fluid domain surrounding the cell as a hemisphere as shown in Figure 3. The size of the domain is determined from numerical simulations of the laminar flow in the whole height of the channel in the presence of an array of spheres adherent to the bottom wall, as performed by Brooks and Tozeren.[31] These authors found that the Poiseuille flow was macroscopically preserved for a sphere radius less than 1/15 of the channel height. They also proved that the bead could be considered to be single, if the separation distance between neighboring beads was larger than 10 times the bead radius. It can be noted that these two requirements are fulfilled in the work described by Mercier-Bonin et al.,[32] the results of which are interpreted in this article. Therefore, the fluid domain surrounding the cell attached to the plate is reduced to a height of 30 cell radii. The size chosen is twice that needed to preserve result accuracy even for nonspherical cell shapes.

Let us consider a fully developed 2-D laminar Poiseuille flow, as has been experimentally demonstrated in the shear stress flow chamber.[20] It is well characterized by the corresponding channel Reynolds number

$$\mathrm{Re}_h = \rho\langle u\rangle h/\mu \tag{1}$$

where h is the half channel height, $\langle u\rangle$, the mean flow velocity, ρ, the density and μ, the dynamic viscosity of the fluid.

The shear rate is uniform and can be expressed as

$$\dot{\gamma} = 3Q/4h^2b \tag{2}$$

with Q, the volumetric flow rate ($Q = 4\langle u\rangle hb$), and b, the channel half width.Using Eqs. 1 and 2, $\mathrm{Re_h}$ can be expressed in terms of $\dot{\gamma}$ as follows

$$\mathrm{Re_h} = \rho\dot{\gamma}h^2/3\mu \tag{3}$$

Taking the chamber half height of 0.1 mm and the maximum shear rate of 10^5 s^{-1}, according to the experiments described by Mercier-Bonin et al.,[32] leads to a channel Reynolds number of about 300. This confirms that the flow is always laminar in the shear stress flow chamber.

Let us now consider the local flow problem giving the velocity u and pressure p in the vicinity of the cell. The flow within the near-wall region can be characterized using the local Reynolds number, based on the radius, r, of the cell and the shear rate at the wall as

$$\mathrm{Re}_c = \rho\dot{\gamma}r^2/\mu \tag{4}$$

where $\dot{\gamma}$ is the shear rate.

It is obvious that $\mathrm{Re_c}$ is always lower than 1, because $r/h \approx 1/100$. It can be concluded that the inertial effects are

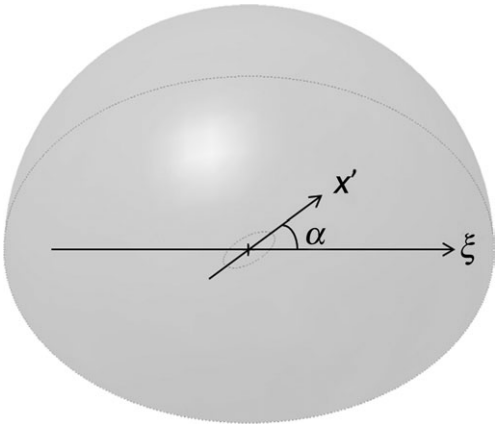

Figure 3. Schematic representation of the hemispherical computational domain surrounding the cell.

negligible in the near-wall region. Consequently, we can make the reasonable assumption that the flow in the near-wall region is governed by the Stokes equations.

The local flow problem is finally described as

$$\nabla \cdot \mathbf{u} = 0 \tag{5}$$

$$\nabla p = \mu \nabla^2 \mathbf{u} \tag{6}$$

A no-slip boundary condition ($\mathbf{u} = 0$) is imposed at the solid boundaries, that is, bottom wall and cell surface. Considering a pure shear $\dot{\gamma}$ in the ζ direction, the fluid velocity far from the cell is imposed on the semispherical boundary.-*Fluid boundary*

$$u_x = \dot{\gamma} z \cos \alpha \tag{7}$$

$$u_y = \dot{\gamma} z \sin \alpha \tag{8}$$

$$u_z = 0 \tag{9}$$

A reference pressure ($p = 0$) is also set at the bottom of the hemisphere.

Computational aspects

The set of equations (5) and (6), with the aforementioned boundary conditions, are solved using COMSOL Multiphysics software. We take advantage of the existence of a contact area between the bacterial cell surface and the flat wall in the real situation to avoid the meshing problems generally encountered when two interacting surfaces make contact in a single point. Here, a line is common to the cell surface and the flat wall. The mesh is refined at the cell surface and progressively coarsened toward the outer boundary. The triangular mesh size varies from 12,000 elements for the sphere-shaped bacteria to 118,000 for the rod-shaped one. A BiCG-Stab method is used to solve the resulting linear system.

Modeling of the adhesion force

Detachment Model. To interpret the shear stress flow chamber-related experimental results in terms of the net adhesion force between a bacterium and a flat plate, it is necessary to determine the relationship between the net adhesion force and the wall shear stress at detachment. To this end, the hydrodynamic forces and torque exerted by fluid flow over the cells have to be known. They will be calculated from the velocity and pressure fields obtained numerically. A detachment model was proposed by Lorthois et al.[20] to quantify the net adhesion force of fibrin-coated spherical latex beads to a fibrin-coated flat surface. The same theoretical approach was then used by Guillemot et al.[8] and Mercier-Bonin et al.[33] to evaluate the adhesion force between the pairs *Saccharomyces cerevisiae* yeast cells/polystyrene and functionalized microbeads/protein-coated stainless steel. In this article, this modeling is also applied. However, the contact area between the cell and the surface is no longer a circular disc but an ellipse or a quasi rectangle for the spheroid or the rod, respectively. Nevertheless, its size still depends on cell and plate surface properties. Let us consider the typical case of *B. cereus* spores, that is, the spheroid-shaped bacteria for which the shear flow induced detachment has been recently described by Mercier-Bonin et al.[32] According to nanomechanical properties of *B. cereus* spores measured by Fernandes et al.,[34] the spore surface can be considered as rigid, so no deformation occurs. Second, the existence of bonds between the substratum and the spore extreme surface defines the contact area, that is, the area where such bonds are present.[35–37] In the present case, we assume that bonds are mediated, at least to some extent, by the external hair-like nap,[38] the filament length of which ranges from 25 to 40 nm.[39] Third, it is postulated that the roughness of stainless steel is low compared to the characteristic thickness l of the filament meshwork binding the spore to the stainless steel. In this model, we assume that the forces exerted on an immobile cell will lead to the detachment, as soon as they overcome a given threshold. The dynamics of bioadhesion is related to ligand–receptor interactions. These are implied in the migration (motility) of cells along a solid surface.[40] In our approach, the timescale associated with the ligand–receptor interactions is assumed to be long compared to the contact time between the cell surface. As a result, once the cell is detached, it is supposed to roll under the effect of the shear flow. However, not all detachment events lead to rolling and whether a cell rolls actually depends on molecular properties of the receptor and ligand as well as the force acting on the bonds.

The schematic view of a cell lying on the surface is presented in Figure 4. In the upper part, a section of the cell in the (ξ, ζ) vertical plane shows the drag force D and the torque $\Gamma_{\eta/R}$ responsible for the rotation in the plane around the point R. For a sphere, the torques $\Gamma_{\xi R}$ and $\Gamma_{\zeta R}$ are null. Thus, all mechanical forces are solely due to the drag force and the torque $\Gamma_{\xi R}$. If rotation occurs, it will take place in the $\xi\zeta$ plane, and it is reasonable to consider that the rotation axis will belong to the contact area. This uniquely defines the point R. The same applies for a spheroid provided that the $\Gamma_{\xi R}$ and $\Gamma_{\zeta R}$ torques are negligible compared to $\Gamma_{\eta R}$. This condition will be verified in "Variation of Drag and Torque with Geometrical Characteristics of the Spheroid" section.

According to Figure 4a, we have

$$\mathrm{OR}^2 = d^2 + (r_a - l)^2 \tag{10}$$

In the case of a spherical cell, a commonly adopted simplification is that l is negligible compared to the size of the cell.[8,20,41] We also make this assumption here. Using the

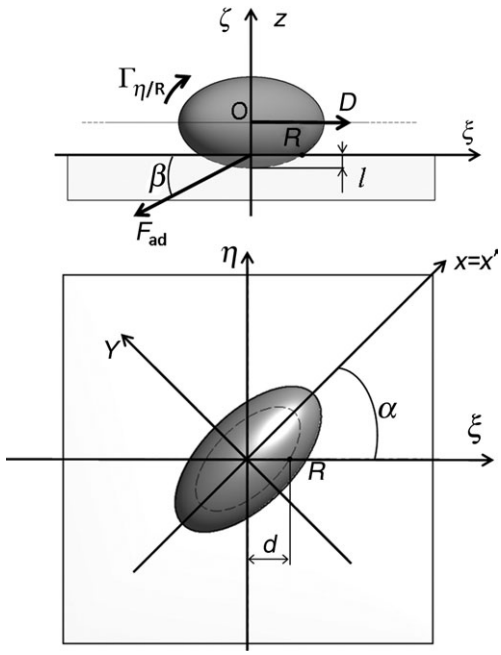

Figure 4. Forces and torque definitions for the spheroid-shaped cell.

geometric properties of the spheroid, we obtain the three following relationships

$$\mathrm{OR} = \sqrt{d^2 + r_a^2\left[1 - \left(\frac{d}{r_b'}\right)^2\right]} \tag{11}$$

$$d = \frac{r_b'}{r_a}\sqrt{2lr_a} \tag{12}$$

$$r_b' = \sqrt{r_b^2\cos^2\alpha + r_a^2\sin^2\alpha} \tag{13}$$

Combining Eqs. 12 and 13 leads to the expression for the apparent contact area radius

$$d = \sqrt{2lr_a\left[\left(\frac{r_b}{r_a}\right)^2\cos^2\alpha + \sin^2\alpha\right]} \tag{14}$$

It can be seen that, in the case of a sphere-shaped model, $r = r_a = r_b$ and the derived expression is

$$d = \sqrt{2lr} \tag{15}$$

If one further assumes that gravity effects and hydrodynamic lift are negligible compared to the drag force, Newton's second law gives[20]

$$F_{adh}\cos\beta = D \tag{16}$$

$$F_{adh}d\sin\beta = \Gamma_{\eta/R} \tag{17}$$

The validity of the latter assumption will be discussed when examining the results of numerical simulations. In these relationships, β is the angle that defines the direction of deformation of the material constituting the sticking layer as depicted in Figure 4. Combining Eqs. 16 and 17 leads to the expression for the net adhesion force

$$F_{ad} = \sqrt{D + \frac{\Gamma_{\eta/R}^2}{d}} \tag{18}$$

The drag and torque in the former equation are dependent on the flow field around the cell. Experimental results provide evidence that the detachment of attached cells is rather a continuous process, as the flow rate in the shear stress flow chamber is increased.[33] In that work, the wall shear stress required to remove 50% of the initially attached cells, denoted $\tau_{W50\%}$, has been proposed as a characteristic parameter for evaluating adhesion strength. Using the values of D and $\Gamma_{\eta/R}$, calculated from the numerical velocity and pressure fields at that wall shear stress ($\tau_{W50\%}$) are used to estimate the net adhesion force.

Particular Case of the Spherical Cell Model. In the ideal case of a laminar infinite linear shear flow over a single spherical particle in contact with an infinite plane, the analytical expressions for the drag (D), torque at sphere center (Γ_0), and lift (L) are given by O'Neill[23] and Krishnan and Leighton[24] as follows

$$D = 32.0\tau_w r^2 + O(\mathrm{Re_c}) \tag{19}$$

$$\Gamma_0 = 11.9\tau_w r^3 + O(\mathrm{Re_c}) \tag{20}$$

$$L = 9.257\tau_w r^2\mathrm{Re_c} \tag{21}$$

where $\tau_w = \mu\dot{\gamma}$ is the wall shear stress. It can be seen that these expressions apply to low local Reynolds number problems. As long as this condition is fulfilled in the present contribution, expressions (19)–(21) will be used to validate the numerical simulation of the flow field.

Experimental Part

AFM experiments were performed to determine the detachment force of *B. cereus* 98/4 spores from stainless steel surfaces. Studies were conducted using a JPK BioMAT Workstation (JPK Instruments AG, Berlin Germany), allowing spores and the AFM cantilever to be optically monitored while operating on a stainless steel sample. We worked in the force vs. distance mode (force curves). All experiments were conducted in liquid medium (bidistilled H_2O) at room temperature. Veeco NP-O tip-less cantilevers were used, with a nominal spring constant of 0.06 N/m; spring constants were calibrated using the thermal noise method integrated in the JPK software. Isolated spores were adsorbed onto tip-less cantilevers (no chemical cross-links). Adhesion curves were obtained upon engagement on different locations of the stainless steel material. Experiment parameters included a force threshold of 1 nN (maximum applied force), a z-range of 3 μm (z-tip displacement), a contact time of 10 s and a cantilever velocity of 3 μm/s. Ten spores were probed using five different cantilevers for a total of 100 force curves recorded.

Results and Discussion

We recall here that we intend to interpret, from a physical point of view, bacterial detachment experiments performed in a shear stress flow chamber in terms of the net adhesion

force, deduced from an accurate calculation of the hydrodynamic stresses exerted on the bacteria. To this end, three different cell shapes are investigated: (i) a sphere for the validation of the numerical model, (ii) a spheroid-shaped bacterium like *B. cereus* spore, frequently isolated in food-processing lines[42,43] and recently characterized in terms of detachment rate from stainless steel under shear flow,[32] and (iii) rod-shaped bacteria like *Listeria monocytogenes*, *Escherichia coli*, and *Pseudomonas aeruginosa*, the three being widely encountered in biofilm-related applications.[44–46] For case (ii), the adhesion force was modeled and then compared with direct AFM measurements. Case (iii) was more particularly focused on the theoretical basis for reorientation under shear flow.

Results are analyzed over a large range of wall shear stresses ($\mathbf{1\,Pa<\tau_w<100\,Pa}$) according to experimental investigations, which corresponds to shear rates varying between 10^3 and 10^5 s^{-1}. It should be noted that a single computation at one particular wall shear rate is sufficient to deduce the results for the whole range of wall shear rates, because the governing equations (5) and (6) and the associated boundary conditions are fully linear.

Sphere-shaped cell model

In this preliminary part of the work, the sphere model is mainly investigated for validation purposes. The first objective is to compare the three simulated hydrodynamic stresses, drag, lift, and torque at sphere center to those determined using the analytical expressions given in the previous section. Although our problem is fully linear, the software imposes the solving of the incompressible Navier Stokes equations.

$$\rho(\mathbf{u}\cdot\nabla)\mathbf{u} = -\nabla p + \mu\nabla^2\mathbf{u} \tag{22}$$

Then, and in that case only, simulations were performed considering the whole range of wall shear rates. The second objective is to check whether the inertial term is negligible in the range of Reynolds numbers considered or not. If so, all forces and torque should be linear functions of the wall shear rate, and the flow could be assumed to be purely viscous. Consequently, a single calculation would be sufficient to determine the stresses on the cell for the whole range of Reynolds numbers.

The sphere model is a sphere of radius 1 μm, with an embedment equal to 1% of the sphere radius. The radius of the resulting contact area is 0.14 μm.

Results in terms of drag, lift, and torque are presented in Figure 5. Calculations lead to accurate results, because the maximum relative error is less than 1.2% for the drag and less than 3.0% for the torque. We also recall that expressions (19)–(21) were deduced from an asymptotic development at the first order in Re_c. This means that they are only accurate, when $Re_c \ll 1$ but is not zero. The range of Reynolds numbers considered in this study is [0.001–0.1], and this probably explains the increasing discrepancy between numerical and analytical values, as the shear rate increases. As far as the lift is concerned, the error increases with the shear rate, reaching 12% at the highest value. This difference can be attributed to the fact that our geometry differs slightly from a sphere on a plane, which has a major influence on the lift force. This error is not detrimental to further analysis, because results also show that the lift force is at least one order of magnitude lower than the drag force. Assuming a cell density equal to twice that of water, the Archimedes's force was estimated at 4.1×10^{-14} N, which is also much smaller than the drag force. Thus, it is verified here that the lift and the gravity forces can be neglected in the detachment mechanisms, as proposed by Lorthois et al.[20]

Spheroid-shaped cell model

Variation of Drag and Torque with Geometrical Characteristics of the Spheroid. We now consider a spheroid with an equatorial radius of 1 μm and a polar radius that is made to vary from 1 to 2 μm ($1<r_b/r_a \leq 2$). The embedment of the spheroid is set between 0.1 and 0.9 μm. The incidence angle α of the main flow direction relative to the symmetry axis of the cell also varies within the range $0 \leq \alpha \leq \pi$. The degree of asymmetry implies the existence of a torque $\Gamma_{\zeta/R}$ in the vertical direction and a torque $\Gamma_{\xi/R}$ in the main incident flow direction when the cell is not facing the flow ($\alpha = 0$ or $\alpha = \pi/2$ or $\alpha = \pi$).

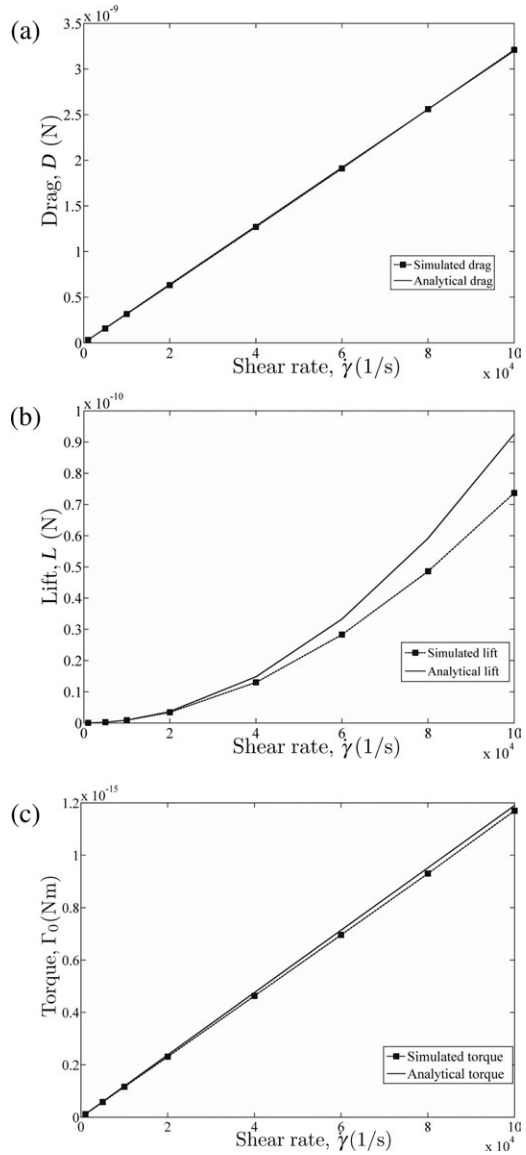

Figure 5. Variation of drag (a), lift (b), and torque (c) acting on a sphere as a function of the shear rate γ (r =1 μm and l = r/10).

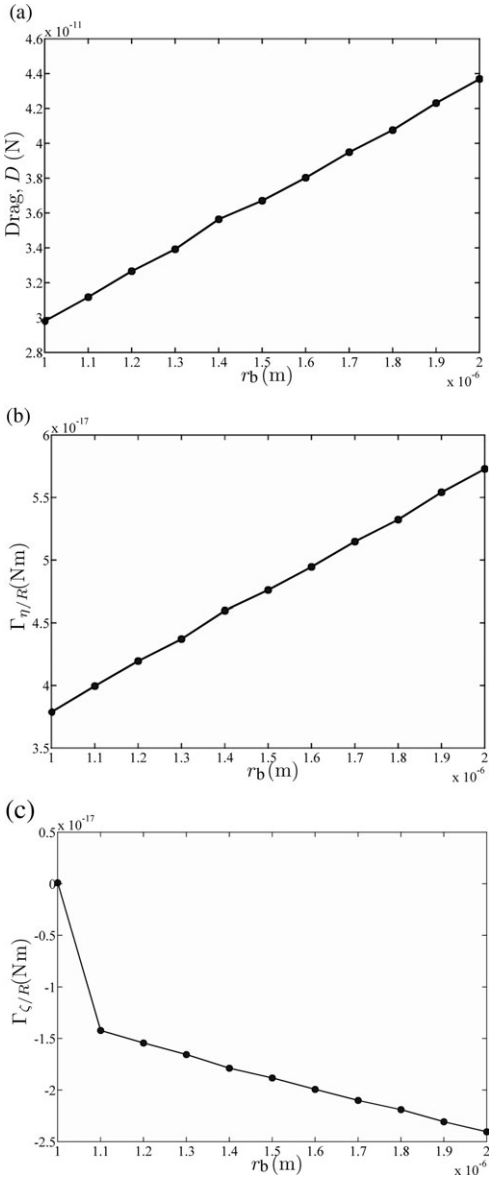

Figure 6. Variation of drag (a) and torque (b and c) for the spheroid-shaped cell model as a function of half the cell length (r_a =1 μm, $l = r_a/10$, $\theta = \frac{\pi}{2}$, $\alpha = \frac{\pi}{4}$, $\gamma = 10^3\ s^{-1}$).

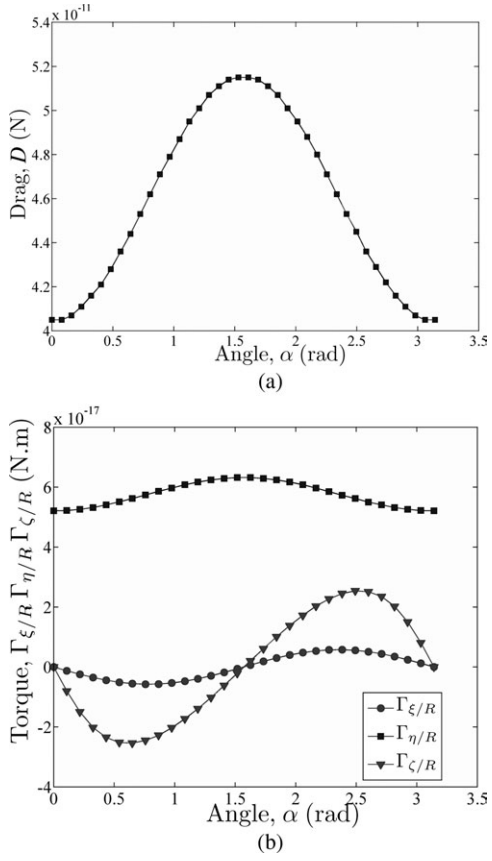

Figure 7. Variation of drag (a) and torque (b) components as a function of the flow incidence angle α for the spheroid-shaped cell model (r_a =1 μm, $r_b = 2r_a$, $l = r_a/10$, $\theta = \frac{\pi}{2}$, $\gamma = 10^3\ s^{-1}$).

Figure 6 displays the change in the drag and in the components $\Gamma_{\eta/R}$ and $\Gamma_{\zeta/R}$ of the torque, when the length of the semimajor axis r_b increases. The influence of the lengthening of r_b/r_a was investigated for an incident angle $\alpha = \pi/4$. That position was chosen, because the $\Gamma_{\zeta/R}$ component of the torque that appears as a consequence of the lengthening is then maximal. The results indicate that the stresses over the spheroid increase linearly with r_b. A 50% increase in the drag and torque component $\Gamma_{\eta/R}$ is observed for $r_b = 2$ μm. Additionally, the component $\Gamma_{\zeta/R}$ is no longer negligible, when the aspect ratio is increased. The third component of the torque $\Gamma_{\xi/R}$ is neglected, because its value is systematically two orders of magnitude lower than the η and ζ components (results not shown).

The influence of the incidence angle α on the drag force is presented in Figure 7a. The relative change between the minimum value, obtained when the major axis is aligned with the flow ($\alpha = 0$), and the maximum value, reached for $\alpha = \pi/2$, is about 25%.

Figure 7b exhibits the three components of the torque as a function of α. Contrary to what occurs with the sphere-shaped cell model, the components of the torque in the ζ and ξ directions are not zero. Nevertheless, $\Gamma_{\eta/R}$ could be expected to be the most significant component of the torque. It is maximum for $\alpha = \pi/2$, minimum for $\alpha = 0$ and is always one order of magnitude higher than the $\Gamma_{\xi/R}$. The components $\Gamma_{\xi/R}$ and $\Gamma_{\zeta/R}$ are maximum for $\alpha = \pi/4$ and equal zero for $\alpha = 0$, $\alpha = \pi/2$, and $\alpha = \pi$. The sign of these torque components means that the prevalent rotation direction of the cell around the ξ and ζ axes depends on the incident angle of the main flow relative to the axis of symmetry of the cell.

This can be related to an experimental analysis previously performed on *B. cereus* spores in a shear stress flow chamber: cell rolling and cell reorientation occurred at the same time, with coexistence of spore rotation and displacement in the direction of the flow.[32]

The embedment of the spheroid is then varied in the range of 10–90% of the spheroid radius. A 90% embedment approaches a cell flattened on the plate or a cell placed in a protrusion. The effect of the embedment is studied for an aspect ratio of the spheroid $r_b/r_a = 2$. Both the drag and the torque Γ_η are drastically reduced, when 90% of the bottom half of the cell is removed (Figure 8).

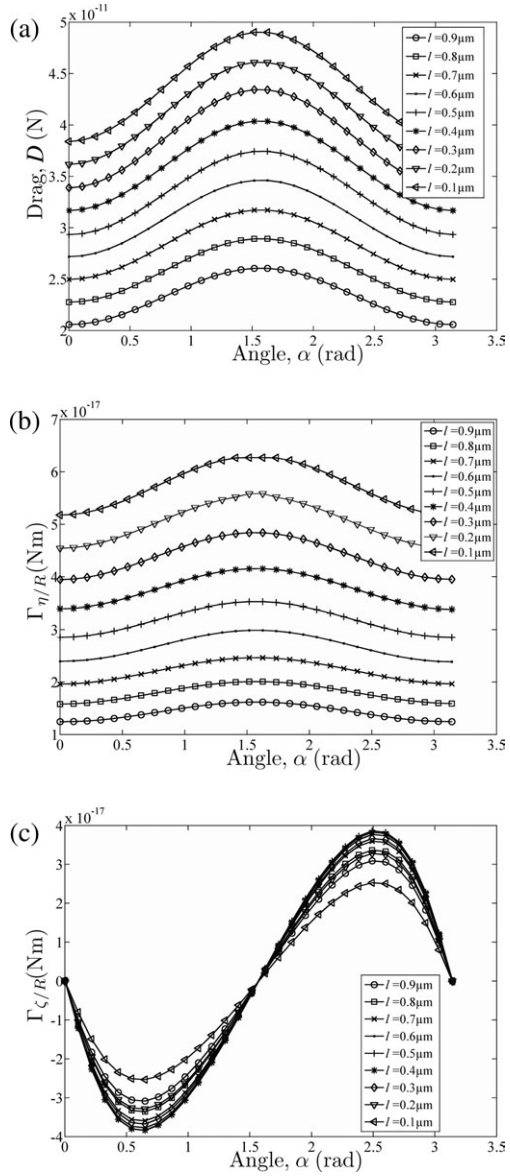

Figure 8. Variation of drag (a) and torque (b and c) components as a function of the orientation α of the spheroid-shaped cell model, for different embedment heights ($r_a = 1$ μm, $r_b = 2r_a$, $\theta = \frac{\pi}{2}$, $\gamma = 10^3$ s^{-1}).

Modeling the Force of Adhesion to Stainless Steel: Comparison with Direct AFM Measurements. Once all the hydrodynamic stresses exerted over the spheroid-shaped bacteria attached to a flat surface have been carefully quantified, the magnitude of the net adhesion force can be determined using equation (18). The shape, size and volume of a spore were deduced from Transmission Electron Microscopy (TEM) observations performed by Faille et al.[39] The spore was well modeled by a spheroid with a polar radius of 0.84 μm and an equatorial radius of 0.4 μm. The corresponding volume was estimated to be 0.56 ± 0.12 μm^3. The characteristic thickness, l, corresponding to the length of filaments constituting the external hair-like nap was taken to be equal to 25 nm. All this information was used to determine the equivalent diameter of the contact area through equation (16).

These data were then used to quantify the adhesion force of *B. cereus* spores to stainless steel, considering the Bc 98/4 strain. To this end, we computed the drag force and torque owing to the wall shear stress required to remove 50% of initially attached cells (24.8 ± 5.5 Pa), as obtained by Mercier-Bonin et al.[32] Under the assumption of the spherical shape investigated in that work, the adhesion force was estimated at 930 pN. Here, a more realistic shape is considered. The resulting adhesion forces (see eq. 18), together with the parameters D, $\Gamma_{\eta/R}$ and d, obtained from equation (14), are given in Table 1 for some particular values of the incident angle α. First of all, it must be pointed out that the values in Table 1 indicate the minimum adhesion force required to prevent the detachment at a given wall shear stress of 24.8 Pa. These values can be extrapolated to another wall shear stress thanks to the linearity of the problem. Should all cells be oriented in the same manner in the experiment, say $\pi/4$, it can be deduced from Table 1 that the adhesion force is about 418 pN. In contrast, if a cell oriented at $\pi/2$ remains attached, it can be concluded that the adhesion force is larger than 694 pN. There are different ways of interpreting these results:

Table 1. Magnitude of the Adhesion Force as a Function of the Flow Incidence Angle

α	D (pN)	$\Gamma_{\eta/R}$ (pN μm)	d (μm)	F_{adh} (pN)
0	140	78	0.28	308
$\pi/6$	151	82	0.25	355
$\pi/4$	161	86	0.22	418
$\pi/3$	171	91	0.19	514
$\pi/2$	180	95	0.14	694

(i) For a given wall shear stress, the adhesion force required to remain attached ranges from 300 to 700 pN depending on the orientation of the cell. These results are in good agreement with the value of 430 pN found for the force needed to detach Bc 98/4 spores from stainless steel, as measured by AFM (Figure 9). Detachment force histograms are provided in Figure 9b, which shows that the force variations due to the bacterial contact surface mobilized (incl. number of binding molecules) also differ from one spore to another. These are all more remarkable, as these two methods are completely different. Indeed, shear flow induced detachment is an indirect method, which is used on the entire bacterial population and requires a detachment model to be stated for rolling and sliding as well as a quantification of the hydrodynamic force and torque exerted on the cell. In contrast, AFM is a direct method that measures the vertical force required for bacteria detachment at single-cell level.

(ii) The hydrodynamic stresses on the cell depend on its orientation. If it is assumed that the adhesion force is constant among the cell population, a preferential detachment should be observed for those cells that are not aligned with the main direction of the flow.

Thus, the detachment probability may result from a combination of both the adhesion force and the orientation relative to the main flow.

Rod-shaped cell model

The rod-shaped cell model aims to mimic adhesive behavior of gram-negative (*E. coli* and *P. aeruginosa*) and gram-positive (*L. monocytogenes*) bacteria, often subjected to shear flow in biomedical and food applications. Early work mentioned the ability of bacteria to be attached by one pole

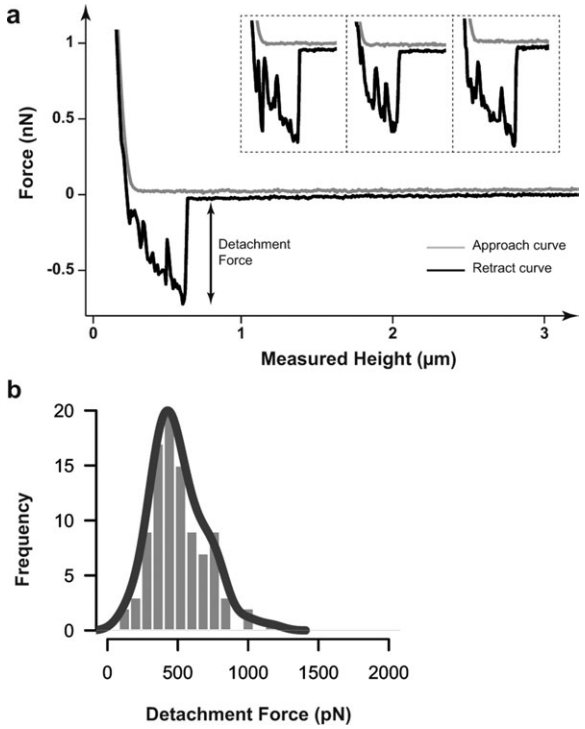

Figure 9. (a) Detachment force curves obtained using AFM. Data show four sample curves of force vs. *z*-measured height during approach (gray) and retraction (black).

The maximum vertical jump seen at retraction gives the force needed for detachment. (b) Detachment force histogram (gray) and probability density function (black) of the numerous recorded force curves. A peak clearly arises around 430 pN.

and rotate.[47] Recent studies have demonstrated the possibility of two remarkably different positions: vertical and horizontal.[26,48] Indeed, bacteria appeared to be attached by one pole or to lie flat on the substrate. Furthermore, some of them tended to rotate and align with the flow, whereas others were permanently misaligned or even perpendicular to the flow.[45]

The rod-shaped cell model consists of two hemispheres joined by a cylinder as depicted in Figure 2c. It should be noted that the model bacterium is attached to the surface by one pole. The effect of zenith angle is investigated by varying θ between 0 (vertical position) and $\pi/2$ (horizontal position). The results plotted in Figure 10 clearly show the drastic effect of the position of the bacterium on the hydrodynamic stresses exerted. Vertical bacteria experience a three-times higher drag and a 10-times higher torque $\Gamma_{\eta/R}$ than bacteria lying on the surface. Whatever the cell orientation (angle α), we should note that values computed for $\theta = 18^\circ$ are slightly above those obtained for $\theta = 0$. In our opinion, these surprising results are most probably caused by a rupture in the flow symmetry in the pole region, which occurs when θ deviates from 0.

The torque around the vertical axis $\Gamma_{\zeta/R}$ equals zero, when the incident angle α is 0 or π and is maximum when α is $\pi/2$, whatever the zenith angle. This behavior is notably different from what was observed for the spheroid-shaped cell model, because no sign change is observed here. This is essentially due to the fact that the rod-like bacterium rotates around one of its poles, whereas the spheroid rotates around

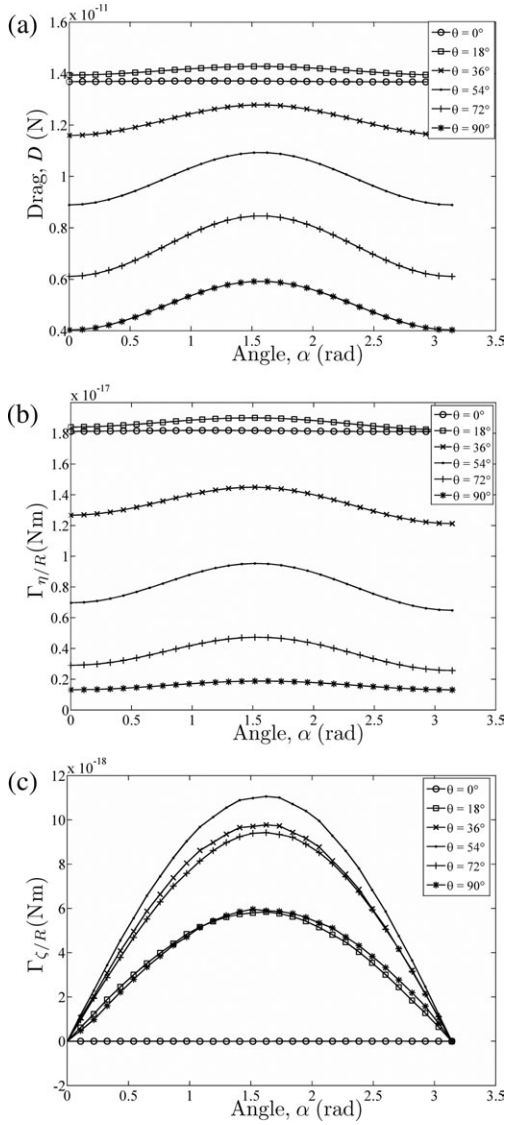

Figure 10. Variation of drag (a) and torque (b and c) components as a function of the orientation α of the rod-shaped cell model for different inclinations θ ($b = 2$ μm, $r = 0.25$ μm, $l = r/10$, $\gamma = 10^3$ s^{-1}).

its vertical axis of symmetry. One can further observe that the torque $\Gamma_{\zeta/R}$ first increases with the zenith angle, peaks for a zenith angle around 54°, and then decreases. Two opposite effects can explain these results: the lever arm increases monotonously with the zenith angle, while the force resulting from the hydrodynamic stresses on the rod surface decreases as the zenith angle increases. The torque $\Gamma_{\zeta/R}$ behaves similarly, though it is less sensitive to the incident angle α.

The variations of the torque around the ξ axis are more complex to interpret, but this component is much lower than the two others. In consequence, it is not expected to play a significant role in the bacteria movement (data not shown). Considering the respective magnitudes of the three torques $\Gamma_{\xi/R}$, $\Gamma_{\eta/R}$, and $\Gamma_{\zeta/R}$, it can be claimed that bacteria remaining attached to the surface at high shear rates should mainly be lying flat and oriented in the main flow direction. This is confirmed by the observations of Lecuyer et al.[45] on *P. aeruginosa* adhered to a glass surface under shear flow. However,

the change in position was mediated by an undetermined number of bonds that could break or rearrange. Similarly, the position of *Xylella fastidiosa* on a glass surface under very low flow rate conditions was seen to be more or less vertical with bacteria being attached at the pilus-bearing pole.[26] As the medium flow was increased, cells tended to gradually lie on the surface and became oriented with the direction of flow. In this framework, in line with our previous observations on the spheroid-shaped cell model (Bc 98/4 spores),[32] we experimentally verified such predicted lying/reorientation under shear flow for rod-shaped bacteria, considering the gram-negative *E. coli* model (unpublished data).

Conclusions

Numerical simulations of the flow field around various objects, representative of typical bacterial shapes, were performed. Calculations of the hydrodynamic stresses exerted over a single sphere by shear flow were in good agreement with the existing analytical solutions. For nonsymmetrical objects (spheroid and rod), the influence of the flow orientation and the aspect ratio was established at moderate computational expense through the use of a parametric solver. When applied to more complex bacterial shapes, the proposed approach provided a more thorough understanding of the most influent parameters governing the shear flow induced detachment of attached cells. Preferential rolling and reorientation of cells, shown experimentally in the literature, were confirmed from a theoretical point of view here. Furthermore, when the spheroid-shaped cell model was applied to *B. cereus* spores, the predicted adhesion force to stainless steel was demonstrated to be of the same order of magnitude as the experimental value, obtained with direct AFM measurements. It can be concluded that the numerical computations developed in this article are very valuable for the quantitative interpretation of shear flow induced detachment experiments in terms of net adhesion force. Sensitivity analysis on various parameters (size, aspect ratio, orientation, and initial position) now offers the possibility to investigate the effects of physicomechanical heterogeneity on the detachment of a cell population.

Acknowledgments

The authors gratefully acknowledge the financial support of the ANR INTERSPORE project.

Literature Cited

1. Ramage G, Martínez JP, López-Ribot JL. Candida biofilms on implanted biomaterials: a clinically significant problem. *FEMS Yeast Res*. 2006;6:979–986.
2. Characklis WG. Attached microbial growths—I. Attachment and growth. *Water Res*. 1973;7:1113–1127.
3. Compère C, Bellon-Fontaine MN, Bertrand P, Costa D, Marcus P, Poleunis C, Pradier CM, Rondot B, Walls MG. Kinetics of conditioning layer formation on stainless steel immersed in seawater. *Biofouling: J Bioadhesion Biofilm Res*. 2001;17:129–145.
4. Briandet R, Meylheuc T, Maher C, Bellon-Fontaine MN. *Listeria monocytogenes* Scott A: cell surface charge, hydrophobicity, and electron donor and acceptor characteristics under different environmental growth conditions. *Appl Environ Microbiol*. 1999;65: 5328–5333.
5. Blel W, Le Gentil-Lelièvre C, Bénézech T, Legrand J, Legentilhomme P. Application of turbulent pulsating flows to the bacterial removal during a cleaning in place procedure. Part 1: Experimental analysis of wall shear stress in a cylindrical pipe. *J Food Eng*. 2009;90:422–432.
6. Blel W, Legentilhomme P, Bénézech T, Legrand J, Le Gentil-Lelièvre C. Application of turbulent pulsating flows to the bacterial removal during a cleaning in place procedure. Part 2: Effects on cleaning efficiency. *J Food Eng*. 2009;90:433–440.
7. Bower CK, McGuire J, Daeschel MA. The adhesion and detachment of bacteria and spores on food-contact surfaces. *Trends Food Sci Technol*. 1996;7:152–157.
8. Guillemot G, Lorthois S, Schmitz P, Mercier-Bonin M. Evaluating the adhesion force between *Saccharomyces cerevisiae* yeast cells and polystyrene from shear-flow induced detachment experiments. *Chem Eng Res Des*. 2007;85:800–807.
9. Saulou C, Despax B, Raynaud P, Zanna S, Marcus P, Mercier-Bonin M. Plasma deposition of organosilicon polymer thin films with embedded nanosilver for prevention of microbial adhesion. *Appl Surf Sci*. 2009;256(3, Suppl 1):S35–S39.
10. Guillemot G, Despax B, Raynaud P, Zanna S, Marcus P, Schmitz P, Mercier-Bonin M. Plasma deposition of silver nanoparticles onto stainless steel for the prevention of fungal biofilms: a case study on *Saccharomyces cerevisiae*. *Plasma Process Polym*. 2008;5:228–238.
11. Leclercq-Perlat MN, Lalande M. Cleanability in relation to surface chemical composition and surface finishing of some materials commonly used in food industries. *J Food Eng*. 1994;23:501–517.
12. Faille C, Jullien C, Fontaine F, Bellon-Fontaine M-N, Slomianny C, Benezech T. Adhesion of *Bacillus spores* and *Escherichia coli* cells to inert surfaces: role of surface hydrophobicity. *Can J Microbiol*. 2002;48:728–738.
13. Rönner U, Husmark U, Henriksson A. Adhesion of bacillus spores in relation to hydrophobicity. *J Appl Microbiol*. 1990;69:550–556.
14. Trache A, Meininger GA. Atomic Force Microscopy (AFM). *Current Protocols in Microbiology*. 2008; 8:2C.2.1-2C.2.17.
15. Castelain M, Pignon F, Piau J-M, Magnin A, Mercier-Bonin M, Schmitz P. Removal forces and adhesion properties of *Saccharomyces cerevisiae* on glass substrates probed by optical tweezer. *J Chem Phys*. 2007;127:135104.
16. Meinders JM, van der Mei HC, Busscher HJ. Physicochemical aspects of deposition of *Streptococcus thermophilus* B to hydrophobic and hydrophilic substrata in a parallel plate flow chamber. *J Colloid Interface Sci*. 1994;164:355–363.
17. Goldstein AS, DiMilla PA. Application of fluid mechanic and kinetic models to characterize mammalian cell detachment in a radial-flow chamber. *Biotechnol Bioeng*. 1997;55:616–629.
18. Detry JG, Rouxhet PG, Boulangé-Petermann L, Deroanne C, Sindic M. Cleanability assessment of model solid surfaces with a radial-flow cell. *Colloids Surf A: Physicochem Eng Aspects*. 2007;302:540–548.
19. Guillemot G, Vaca-Medina G, Martin-Yken H, Vernhet A, Schmitz P, Mercier-Bonin M. Shear-flow induced detachment of *Saccharomyces cerevisiae* from stainless steel: influence of yeast and solid surface properties. *Colloids Surf B: Biointerfaces*. 2006;49:126–135.
20. Lorthois S, Schmitz P, Anglés-Cano E. Experimental study of fibrin/fibrin-specific molecular interactions using a sphere/plane adhesion model. *J Colloid Interface Sci*. 2001;241:52–62.
21. Mercier-Bonin M, Ouazzani K, Schmitz P, Lorthois S. Study of bioadhesion on a flat plate with a yeast/glass model system. *J Colloid Interface Sci*. 2004;271:342–350.
22. Bakker DP, van der Plaats A, Verkerke GJ, Busscher HJ, van der Mei HC. Comparison of velocity profiles for different flow chamber designs used in studies of microbial adhesion to surfaces. *Appl Environ Microbiol*. 2003;69:6280–6287.
23. O'Neill ME. A sphere in contact with a plane wall in a slow linear shear flow. *Chem Eng Sci*. 1968;23:1293–1298.
24. Krishnan GP, Leighton DT. Inertial lift on a moving sphere in contact with a plane wall in a shear flow. *Phys Fluids*. 1995;7:2538–2546.
25. Cantat I, Misbah C. Lift force and dynamical unbinding of adhering vesicles under shear flow. *Phys Rev Lett*. 1999;83:880–883.
26. De La Fuente L, Montanes E, Meng Y, Li Y, Burr TJ, Hoch HC, Wu M. Assessing adhesion forces of type I and type IV pili of *Xylella fastidiosa* bacteria by use of a microfluidic flow chamber. *Appl Environ Microbiol*. 2007;73:2690–2696.
27. Olivier LA, Truskey GA. A numerical analysis of forces exerted by laminar flow on spreading cells in a parallel plate flow chamber assay. *Biotechnol Bioeng*. 1993;42:963–973.
28. Gaver DP, Kute SM. A theoretical model study of the influence of fluid stresses on a cell adhering to a microchannel wall. *Biophys J*. 1998;75:721–733.
29. Chisti Y. Hydrodynamic damage to animal cells. *Crit Rev Biotechnol*. 2001;21:67–110.
30. Sugihara-Seki M, Schmid-Schönbein GW. The fluid shear stress distribution on the membrane of leukocytes in the microcirculation. *J Biomech Eng*. 2003;125:628–638.

31. Brooks SB, Tozeren A. Flow past an array of cells that are adherent to the bottom plate of a flow channel. *Comput Fluids*. 1996;25:741–757.
32. Mercier-Bonin M, Dehouche A, Morchain J, Schmitz P. Orientation and detachment dynamics of *Bacillus* spores from stainless steel under controlled shear flow: modelling of the adhesion force. *Int J Food Microbiol*. 2011; 146(2):182–191.
33. Mercier-Bonin M, Adoue M, Zanna S, Marcus P, Combes D, Schmitz P. Evaluation of adhesion force between functionalized microbeads and protein-coated stainless steel using shear-flow-induced detachment. *J Colloid Interface Sci*. 2009;338:73–81.
34. Fernandes JC, Eaton P, Gomes AM, Pintado ME, Xavier Malcata F. Study of the antibacterial effects of chitosans on *Bacillus cereus* (and its spores) by atomic force microscopy imaging and nanoindentation. *Ultramicroscopy*. 2009;109:854–860.
35. Hammer DA, Lauffenburger DA. A dynamical model for receptor-mediated cell adhesion to surfaces. *Biophys J*. 1987;52:475–487.
36. Cozens-Roberts C, Quinn JA, Lauffenburger DA. Receptor-mediated cell attachment and detachment kinetics. II. Experimental model studies with the radial-flow detachment assay. *Biophys J*. 1990;58:857–872.
37. Kuo SC, Lauffenburger DA. Relationship between receptor/ligand binding affinity and adhesion strength. *Biophys J*. 1993;65:2191–2200.
38. Brahmbhatt TN, Janes BK, Stibitz ES, Darnell SC, Sanz P, Rasmussen SB, O'Brien AD. *Bacillus anthracis* exosporium protein bclA affects spore germination, interaction with extracellular matrix proteins, and hydrophobicity. *Infect Immun*. 2007;75:5233–5239.
39. Faille C, Lequette Y, Ronse A, Slomianny C, Garénaux E, Guerardel Y. Morphology and physico-chemical properties of *Bacillus* spores surrounded or not with an exosporium: consequences on their ability to adhere to stainless steel. *Int J Food Microbiol*. 2010;143:125–135.
40. Sarvestani AS, Jabbari E. Modeling cell adhesion to a substrate with gradient in ligand density. *AIChE J*. 2009;55:2966–2972.
41. Décavé E, Demilly M, Fourcade B, Bruckert F, Boulangé L, Brechet Y. Biological cell detachment kinetics from an inert substrate. *Philos Mag*. 2005;85:3173–3189.
42. Flint SH, Bremer PJ, Brooks JD. Biofilms in dairy manufacturing plant. Description, current concerns and methods of control. *Biofouling: J Bioadhesion Biofilm Res*. 1997;11:81–97.
43. Tauveron G, Slomianny C, Henry C, Faille C. Variability among *Bacillus cereus* strains in spore surface properties and influence on their ability to contaminate food surface equipment. *Int J Food Microbiol*. 2006;110:254–262.
44. Lebert I, Leroy S, Talon R. Effect of industrial and natural biocides on spoilage, pathogenic and technological strains grown in biofilm. *Food Microbiol*. 2007;24:281–287.
45. Lecuyer S, Rusconi R, Shen Y, Forsyth A, Vlamakis H, Kolter R, Stone HA. Shear stress increases the residence time of adhesion of *Pseudomonia aeruginosa*. *Biophys J*. 2011;100:341–350.
46. Tresse O, Shannon K, Pinon A, Malle P, Vialette M, Midelet-Bourdin G. Variable adhesion of *Listeria monocytogenes* isolates from food-processing facilities and clinical cases to inert surfaces. *J Food Prot*. 2007;70:1569–1578.
47. Sjoblad RD, Doetsch RN. Adsorption of polarly flagellated bacteria to surfaces. *Curr Microbiol*. 1982;7:191–194.
48. Agladze K, Wang X, Romeo T. Spatial periodicity of *Escherichia coli* K-12 biofilm microstructure initiates during a reversible, polar attachment phase of development and requires the polysaccharide adhesin PGA. *J Bacteriol*. 2005;187:8237–8246.

Manuscript received Apr. 22, 2011, and revision received Dec. 15, 2011.